Phase-Shift Studies of the Quenching of NH($c^1\Pi$) and NH($A^3\Pi$) by Hydrocarbons

Shun-ichiro SASAKI, Akiko KANO, Shigeru TSUNASHIMA,* and Shin SATO†
Department of Applied Physics, Tokyo Institute of Technology, Ookayama, Meguro-ku, Tokyo 152
†Research Laboratory for Nuclear Reactors, Tokyo Institute of Technology, Ookayama, Meguro-ku, Tokyo 152
(Received December 26, 1985)

The cross-sections for quenching NH($c^1\Pi$) and NH($A^3\Pi$) by hydrocarbons were determined at room temperature by using a phase-shift method. The NH($c^1\Pi$) was produced by the photolysis of HN_3 using an amplitude-modulated Xe-resonance lamp. The apparent decay rate of the NH($c^1\Pi$) was estimated from the difference in phase angle between the excitation light and the fluorescence of NH($c^1\Pi$) at 325 nm. In the presence of Xe, the fluorescence of NH($A^3\Pi$) at 336 nm was enhanced. The difference in the phase angle between the fluorescences at 325 and 336 nm was found to correlate with the decay rate of NH($A^3\Pi$). From the decay rates obtained in the presence of hydrocarbons, the quenching cross-sections were determined.

The NH radical is known to be an important intermediate in astronomical emission sources. The electron configuration, $(2s\sigma)^2(2p\sigma)^2(2p\pi)^2$, of the NH radical gives rise to the $X^3\Sigma^-$, $a^1\Delta$, and $b^1\Sigma^+$ states, while the $(2s\sigma)^2(2p\sigma)(2p\pi)^3$ configuration gives rise to the $c^1\Pi$ and $A^3\Pi$ states. Figure 1 shows a correlation diagram of the NH radical and the O atom. Many similarities have been found in the reactions of NH radicals in the first excited state, NH($a^1\Delta$), with those of isoelectronic species, O(^{1}D) and $CH_2(^1A_1)$.[1-11] The measurements of the quenching processes of these excited states are important in elucidating the mechanism of the energy transfer. The rate constants of the reaction of the NH($a^1\Delta$) state with various molecules have been measured by McDonald et al.[10] and Piper et al.[11] Carrington and his co-workers[12] and Zetsch and Stuhl[13] have determined the rate constants of the quenching of the NH($b^1\Sigma^+$) state by several molecules and found that the NH($b^1\Sigma^+$) state is less reactive than NH($a^1\Delta$), although the former is energetically higher than the latter. This trend is similar to that observed in the case of O(^{1}D);[14] i.e., O(^{1}D) is more reactive than O(^{1}S), although the former is about 200 kJ mol^{-1} energetically lower than the latter. A limited number of quenching rates for the NH($c^1\Pi$) and NH($A^3\Pi$) states have been reported.[15-20] Recent studies of NH($A^3\Pi$) by Hofzumahaus and Stuhl have shown that the NH($A^3\Pi$) was quenched by every three collisions and that the quenching cross-sections of many inorganic molecules were correlated with the intermolecular well depth.[19] No systematic studies of the quenching of these highly excited states by hydrocarbons have been reported, probably because these quencher molecules absorb the vuv light and decompose. One our previous paper showed that the phase-shift method is a convenient and suitable method for the measurements of the quenching rate, especially for a quencher which absorbs the excitation light.[20] In this paper, the cross-sections for the quenching of NH($c^1\Pi$) and NH($A^3\Pi$) by hydrocarbons are reported and possible quenching mechanisms are discussed.

Experimental

The experimental method has been fully described in the previous paper,[20] and so only a brief outline will be given here.

The apparatus consists of an amplitude-modulated Xe-resonance lamp, an oxygen shutter, and a fluorescence cell. The oxygen shutter, which separates the lamp from the cell, was used to cut off the light of wavelengths shorter than 200 nm during the mixing of the reactants and the stabilizing of the lamp before irradiation. The transmitted vuv light was converted to longer wavelengths by using sodium salicylate and was measured at 415.5 nm. The phase angles of the

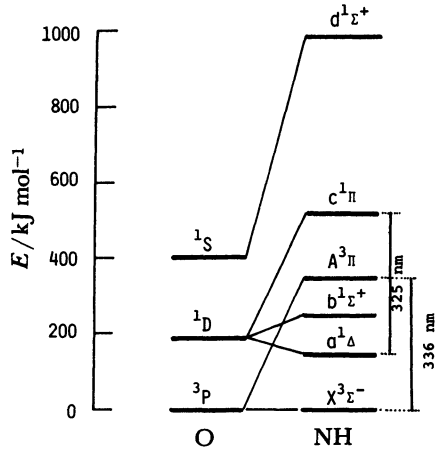

Fig. 1. Correlation diagram of NH and O.

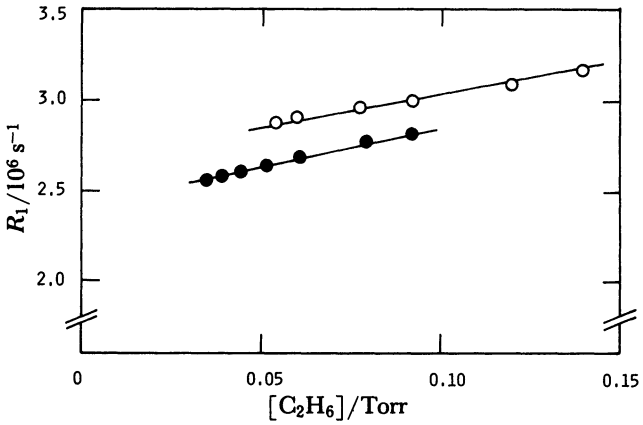

Fig. 2. Plots of R_1 against the pressure of C_2H_6 obtained at f=100 kHz and [He]=20 Torr. ○: [HN_3]= 0.123 Torr, ●: [HN_3]=0.081 Torr.

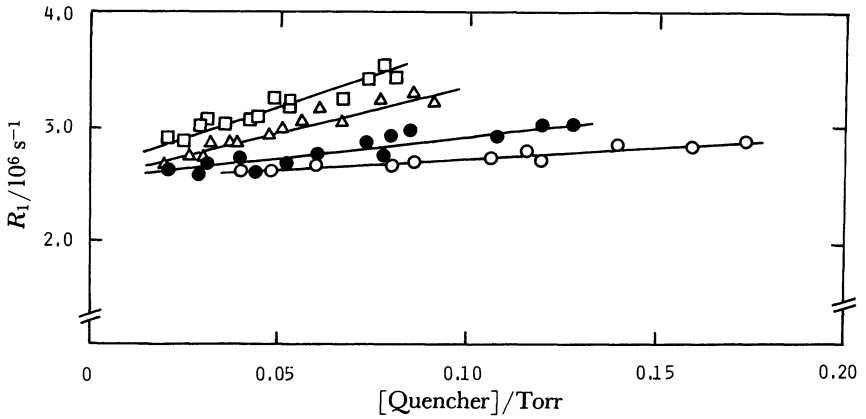

Fig. 3. Plots of R_1 against the pressure of a quencher obtained at f=100 kHz, [HN_3]=0.123 Torr, and [He]=20 Torr. ○: CH_4, ●: c-C_3H_6, △: C_3H_8, □: i-C_4H_{10}.

Table 1. Rate Constants and Cross-Sections for Quenching NH($c^1\Pi$) and NH($A^3\Pi$)[a]

	Quencher	k_{1q}[b]	σ_{1q}[c]	k_{3q}[b]	σ_{3q}[c]
1	CH_4	0.35±0.10	6.5	0.45±0.10	8.3
2	C_2H_6	0.86±0.11	18.1	1.13±0.12	23.9
3	C_3H_8	1.67±0.20	37.4	1.50±0.17	33.6
4	c-C_3H_6	0.75±0.10	16.7	0.88±0.09	19.5
5	n-C_4H_{10}	1.89±0.14	43.7	1.93±0.20	44.6
6	i-C_4H_{10}	1.94±0.29	44.8	1.83±0.15	42.3
7	C_2H_4	2.88±0.30	60.2	1.19±0.09	24.9
8	C_3H_6	2.65±0.20	58.9	1.84±0.11	40.9
9	1-C_4H_8	3.23±0.18	74.3	2.16±0.13	49.7
10	i-C_4H_8	3.19±0.11	73.4	3.50±0.22	80.5
11	t-Δ^2-C_4H_8	3.11±0.13	71.6	3.52±0.14	81.0
12	c-Δ^2-C_4H_8	3.24±0.18	74.6	3.59±0.18	82.6

a) The error limits are one standard deviation. b) In units of 10^{14} cm^3 mol^{-1} s^{-1}. c) $\sigma_q=k_q(\pi\mu/8kT)^{1/2}$, in units of 10^{-16} cm^2.

transmitted light and the fluorescence of the NH radicals were measured by using a lock-in amplifier relative to its reference signal.

Hydrogen azide was synthesized from sodium azide and stearic acid and purified by the method described in the previous paper.[20] Research-grade hydrocarbons were used after several distillations at low temperatures.

Results

Quenching of NH($c^1\Pi$). When a small amount of ethane was introduced into the reactant (0.1—0.3 Torr of HN_3 and 20 Torr of He: 1 Torr=133.3 Pa), the phase difference between the transmitted light and the fluorescence at 325 nm, ϕ_1, decreased. Figure 2 shows the plots of $R_1(=2\pi f/\tan\phi_1)$ as a function of the pressure of ethane. Here, f denotes the frequency of the modulation of the lamp. As is shown in Fig. 2, the plots give straight lines with the same slope for different initial pressures of HN_3. The intercepts increased with an increase in the pressure of HN_3. Similar plots were obtained with other quenchers, such as CH_4, C_3H_8, c-C_3H_6, n-C_4H_{10}, i-C_4H_{10}, C_2H_4, C_3H_6, 1-C_4H_8, i-C_4H_8, and *cis*- and *trans*-Δ^2-C_4H_8. All of the plots gave

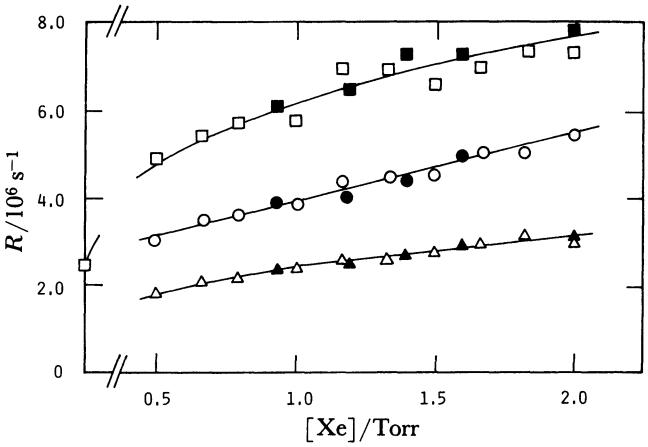

Fig. 4. Plots of R_1, R_3, and R_{13} against the pressure of Xe obtained at [HN_3]=0.07 Torr, and [He]=20 Torr. □: R_1, △: R_3, ○: R_{13}. Open symbols: f=100 kHz, closed symbols: f=120 kHz. The solid lines are calculated ones using Eqs. 18—20. For detail, see Text.

straight lines for every quencher examined. Some examples are shown in Fig. 3. The values of slope of each straight line are summarized in the third column of Table 1. The error limits show one standard deviation.

Effect of Xe on Fluorescence of NH. When Xe was added to a HN_3–He mixture, the intensity of the fluorescence of NH($c^1\Pi$) at 325 nm, decreased while that of NH($A^3\Pi$) at 336 nm increased. The phase-angle difference between the transmitted light and the emission at 336 nm, ϕ_3, was measured, like ϕ_1, at various pressures of HN_3 and Xe. The values of $R_1(=2\pi f/\tan\phi_1)$, $R_{13}(=2\pi f/\tan(\phi_1-\phi_3))$, and $R_3(=2\pi f/\tan\phi_3)$ are plotted as functions of the pressure of Xe in Fig. 4 and of that of HN_3 in Fig. 5.

Effect of Hydrocarbons on R_{13}. The phase-angle difference between the fluorescence of NH($c^1\Pi$) and that of NH($A^3\Pi$), $\phi_1-\phi_3$, was measured in the presence of hydrocarbon in a mixture of He(20 Torr)–HN_3(0.1 Torr)–Xe(0.7 Torr). The plots of R_{13} against the

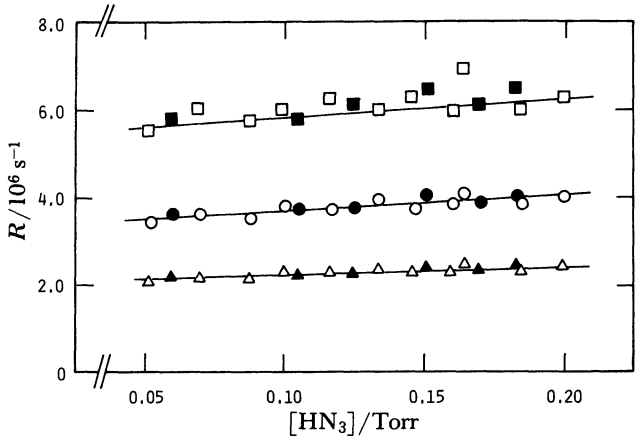

Fig. 5. Plots of R_1, R_3, and R_{13} against the pressure of HN_3 obtained at [Xe]=0.7 Torr, and [He]=20 Torr. For the other conditions, see footnote of Fig. 4.

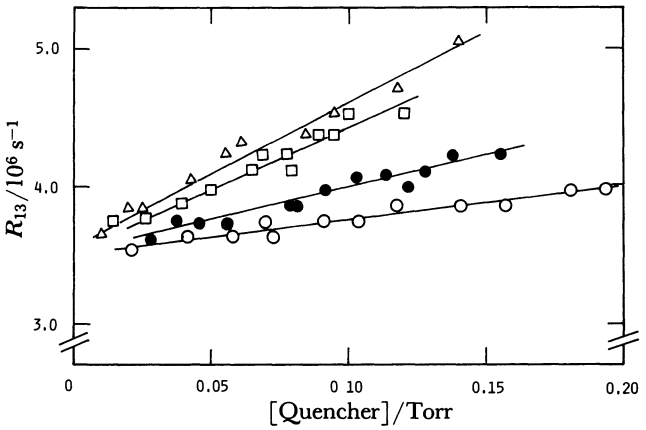

Fig. 6. Plots of R_{13} against the pressure of a quencher obtained at f=100 kHz, $[HN_3]$=0.1 Torr, [Xe]= 0.7 Torr and [He]=20 Torr. ○: CH_4, ●: c-C_3H_6, □: C_3H_8, △: i-C_4H_{10}.

pressure of hydrocarbon gave a straight line for every quencher examined. Some examples are shown in Fig. 6. The values of the slopes of the straight lines are summarized in the fifth column of Table 1.

Discussion

Quenching of NH(c¹Π) by Hydrocarbons. As was discussed in the previous paper,[20] the following reaction mechanism can be considered to explain the results shown in Figs. 2 and 3:

$$HN_3 + h\nu \longrightarrow NH(c^1\Pi) + N_2 \quad (1)$$

$$NH(c^1\Pi) \longrightarrow NH(a^1\Delta) + h\nu(325) \quad k_{10} \quad (2)$$

$$NH(c^1\Pi) + M \longrightarrow \text{products} \quad k_{1M} \quad (3)$$

where M denotes He, HN_3, or hydrocarbons.

Assuming the above reaction mechanism, the following relation can be derived for R_1:

$$R_1 = 2\pi f/\tan\phi_1 \quad (4)$$

$$= k_{10} + k_{1h}[He] + k_{1a}[HN_3] + k_{1q}[Q] \quad (5)$$

where k_{1h}, k_{1a}, and k_{1q} represent k_{1M} for He, HN_3, and the hydrocarbon used respectively. Under constant pressures of He and HN_3, the intercepts of the straight lines in Fig. 3 should be equal to $k_{10}+k_{1h}[He]+k_{1a}[HN_3]$. This R_1 value can be estimated to be $(2.3\pm0.4)\times10^6\ s^{-1}$ by using the previously obtained values of k_{10}, k_{1a}, and k_{1h} under the present experimental conditions; this value is in good agreement with the intercepts obtained in the present studies. Thus, the slope of the straight line shown in Table 1 corresponds to the value of k_{1q}. The quenching cross-sections were calculated from k_{1q} and are summarized in the fourth column of Table 1.

Effect of Xe. The results shown in Figs. 4 and 5 could not be explained by the addition of the following reactions to Reactions 1—3:

$$NH(c^1\Pi) + Xe \longrightarrow NH(A^3\Pi) + Xe \quad k_{1x} \quad (6)$$

followed by:

$$NH(A^3\Pi) \longrightarrow NH(X^3\Sigma^-) + h\nu(336) \quad k_{30} \quad (7)$$

$$NH(A^3\Pi) + M \longrightarrow \text{products} \quad k_{3M} \quad (8)$$

where M denotes a quencher such as He, HN_3, or Xe. If this mechanism is applicable, the following relation should hold for R_1:

$$R_1 = k_{10} + k_{1h}[He] + k_{1a}[HN_3] + k_{1x}[Xe] \quad (9)$$

That is, the plots of R_1 against the pressure of Xe should show a straight line with an intercept of $k_{10}+k_{1h}[He]+k_{1a}[HN_3]$, which is equal to $2.3\times10^6\ s^{-1}$ under the present experimental conditions. As is shown in Fig. 4, this is not the case. In order to explain the present results, then, the following reactions were considered in addition to Reactions 1—3 and 6—8:

$$Xe + h\nu(129.5) \longrightarrow Xe(^1P_1) \quad (10)$$

$$Xe + h\nu(147) \longrightarrow Xe(^3P_1) \quad (11)$$

$$Xe(^1P_1) \longrightarrow Xe + h\nu(129.5) \quad k_{20} \quad (12)$$

$$Xe(^1P_1) + HN_3 \longrightarrow Xe + NH(c^1\Pi) + N_2 \quad k_{2a} \quad (13)$$

$$Xe(^1P_1) + M \longrightarrow \text{products} \quad k_{2M} \quad (14)$$

$$Xe(^3P_1) \longrightarrow Xe + h\nu(147) \quad k'_{20} \quad (15)$$

$$Xe(^3P_1) + HN_3 \longrightarrow Xe + NH(A^3\Pi) + N_2 \quad k'_{2a} \quad (16)$$

$$Xe(^3P_1) + M \longrightarrow \text{products} \quad k'_{2M} \quad (17)$$

The spin-conservation rule was assumed to hold for Reactions 13 and 16.[21] Assuming the above reactions, the following relations were derived:

$$R_1 = AB/(A+B) \quad (18)$$

$$R_3 = (1/A+1/B+1/C)^{-1} \quad (19)$$

$$R_{13} = C \quad (20)$$

Here,

$$A = k_{10} + k_{1h}[He] + k_{1a}[HN_3] + k_{1x}[Xe] \quad (21)$$

$$B = k_{20} + k_{2a}[HN_3] \quad (22)$$

$$C = k_{30} + k_{3h}[He] + k_{3a}[HN_3] + k_{3x}[Xe] \quad (23)$$

where k_{3h}, k_{3a}, and k_{3x} represent k_{3M} for He, HN_3, and Xe respectively. To derive Eqs. 18—20, the following assumptions were made; (i) in the presence of Xe, the direct photolysis of HN_3 was negligible, (ii) the values of A, B, and C were larger than $2\pi f$, and (iii) $k'_{2a}[Xe(^3P_1)]$ was negligibly small compared with $k_{2a}[NH(c^1\Pi)]$ under the present experimental conditions.

From the slopes of the straight lines in the plots of R_{13} vs. $[HN_3]$ and [Xe], the values of k_{3a} and k_{3x} were estimated to be $(6.0\pm1.1)\times10^{13}$ and $(2.8\pm0.1)\times10^{13}$ cm^3 mol^{-1} s^{-1} respectively. The latter value agreed well with that obtained by Hofzumahaus and Stuhl.[19] From the intercepts, the lifetime of $NH(A^3\Pi)$, $1/k_{30}$, was estimated to be 490 ± 40 ns using the value of $k_{3h}=4\times10^{10}$ cm^3 mol^{-1} s^{-1}.[19] The correction by the quenching of He at 20 Torr was less than 0.5%. The lifetime of $NH(A^3\Pi)$ estimated here agrees well with the literature value.[22] The solid lines in Figs. 4 and 5 are drawn by using Eqs. 18—20 with these values: $k_{10}+k_{1h}[He]=2.2\times10^6$ s^{-1}, $k_{1a}=5.2\times10^{13}$ cm^3 mol^{-1} s^{-1},[20] $k_{20}=2.1\times10^6$ s^{-1}, $k_{2a}=2.4\times10^{14}$ cm^3 mol^{-1} s^{-1}, and $k_{1x}=2.2\times10^{14}$ cm^3 mol^{-1} s^{-1}. Although the latter three values are not unique, the agreement is satisfactory, as Figs. 4 and 5 show.

Quenching of $NH(A^3\Pi)$ by Hydrocarbons. When a hydrocarbon is added to the He–HN_3–Xe mixture as a quencher, the following quenching reactions should be considered:

$$NH(c^1\Pi) + Q \longrightarrow \text{products} \qquad k_{1q} \quad (24)$$

$$NH(A^3\Pi) + Q \longrightarrow \text{products} \qquad k_{3q} \quad (25)$$

$$Xe(^1P_1) + Q \longrightarrow \text{products} \qquad k_{2q} \quad (26)$$

$$Xe(^3P_1) + Q \longrightarrow \text{products} \qquad k'_{2q} \quad (27)$$

By the addition of the above reactions, the terms of $k_{1q}[Q]$, $k_{2q}[Q]$, and $k_{3q}[Q]$ should be added to A, B, and C respectively. Under constant pressures of He, HN_3, and Xe, the following relation can be obtained:

$$R_{13} = 2\pi f/\tan(\phi_1-\phi_3) = C_0 + k_{3q}[Q] \quad (28)$$

where C_0 represents the R_{13} values in the absence of the quencher. That is, the slope of the straight line in Fig. 6 represents the k_{3q}. The cross-sections for quenching $NH(A^3\Pi)$, σ_{3q}, were calculated from the values of k_{3q}; they are listed in the sixth column of Table 1.

Comparison with Literature Values. No values have been reported for the cross-sections for quenching $NH(c^1\Pi)$ by hydrocarbons. For the quenching of $NH(A^3\Pi)$ by CH_4, the present results agree well with those obtained by Nishi et al.[17] and Hofzumahaus and Stuhl,[19] although the experimental methods are different.

Collision Complex Model. Recently, Hofzumahaus and Stuhl have measured the cross-sections for the quenching of $NH(A^3\Pi)$ by NH_3, NO, CH_4, H_2, CO, Xe, O_2, CO_2, Ar, N_2, and He, using the laser photolysis of NH_3. They found that the trend of the quenching cross-sections can be described by Parmenter's correlation, which suggests that the attractive force is effective for the quenching process.[19] In Parmenter's correlation, the quenching cross-sections, σ, are correlated with the intermolecular well depth, ε_{qq}:[23]

$$\ln\sigma = \ln C + \beta(\varepsilon_{qq}/k)^{1/2} \quad (28)$$

Here, $\beta=(\varepsilon_{A^*A^*}/kT^2)^{1/2}$, where $\varepsilon_{A^*A^*}$ is the well depth between the excited molecules, A*. Figures 7 and 8 show the plots for the quenching of $NH(A^3\Pi)$ and $NH(c^1\Pi)$ respectively by hydrocarbons. The numbers in Figs. 7 and 8 correspond to the compounds listed in Table 1. The well depth was approximated by $\varepsilon_{qq}/k=1.15\,T_b$, where T_b represents the boiling point.[24] The broken line in Fig. 7 shows the correlation obtained by Hofzumahaus and Stuhl. A good correlation is obtained for the quenching of $NH(A^3\Pi)$ by hydrocarbons:

$$\ln\sigma = (-1.2\pm0.8) + (0.30\pm0.05)(\varepsilon_{qq}/k)^{1/2} \quad (29)$$

The value of the slope is almost the same as that determined by Hofzumahaus and Stuhl.[19] The broken line in Fig. 8 is drawn by using Eq. 29. As is shown in Fig. 8, the trend of the cross-sections of paraffin for quenching $NH(c^1\Pi)$ is different from that of olefin, but it is similar to the case of the quenching of $NH(A^3\Pi)$. The quenching mechanism for olefin should be different from that of paraffin.

Following the method described by Hofzumahaus and Stuhl,[19] absolute cross sections were calculated. The method will be described here only briefly. The interaction potentilal, $V(r)$, is assumed to be in the form of Eq. 30:

$$V(r) = -C_3/r^3 - C_6/r^6 - C_6'/r^6, \quad (30)$$

where the C_3, C_6, and C_6' coefficients represent dipole–dipole ($C_3=2\mu_1\mu_2$), dipole-induced dipole ($C_6=2(\mu_1^2\alpha_2+\mu_2^2\alpha_1)$, and dispersion ($C_6'=1.5I_1I_2\alpha_1\alpha_2/(I_1+I_2)$) interactions respectively. The symbols μ, α, and I represent the dipole moment, the polarizability, and the ionization potential respectively. The effective potential, $V_{eff}(r)$, is given by Eq. 31 at the initial kinetic energy of E and the impact parameter of b:

$$V_{eff}(r) = V(r) + Eb^2/r^2 \quad (31)$$

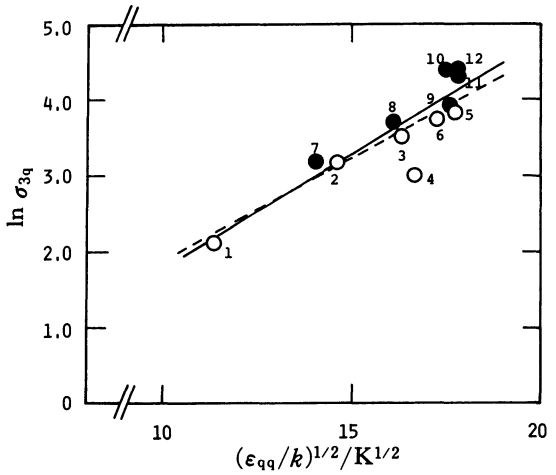

Fig. 7. Plots of $\ln\sigma_{3q}$ against $(\varepsilon_{qq}/k)^{1/2}$ for the quenching of NH(A³Π). The numbers correspond to the compound listed in Table 1. O: paraffin, ●: olefin. The broken line shows the relation, $\ln\sigma=-0.82+0.275\,(\varepsilon_{qq}/k)^{1/2}$.[19]

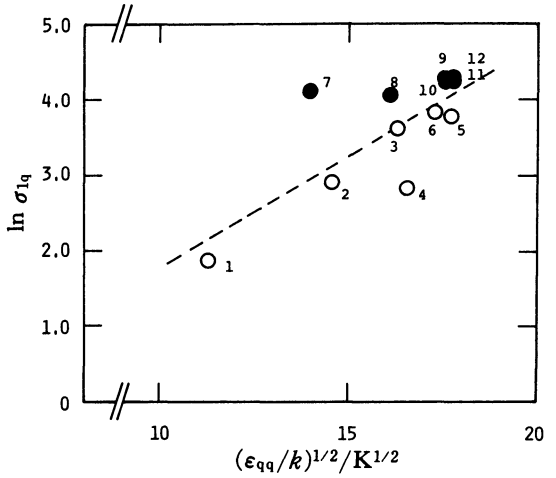

Fig. 8. Plots of $\ln\sigma_{1q}$ against $(\varepsilon_{qq}/k)^{1/2}$ for the quenching of NH(c¹Π). The numbers correspond to the compound listed in Table 1. The broken line represents the best fit line obtained for the quenching of NH(A³Π).

The position of the centrifugal maximum, r_0, can be estimated, by the use of Eq. 32, as a function of E, where the orbiting condition, $E=V_{eff}(r_0)$, is satisfied:

$$\partial V_{eff}(r)/\partial r = 0 \quad \text{at } r = r_0 \tag{32}$$

Thus, the cross-section at the initial kinetic energy of E can be estimated by $\sigma(E)=\pi b^2=\pi r_0^2(1-V(r_0)/E)$. Thus, the thermally averaged cross-section, $\sigma(T)$, can be estimated by Eq. 33:

$$\sigma(T) = (1/kT)^2\int\sigma(E)\,E\exp(-E/kT)\mathrm{d}E \tag{33}$$

In Table 2, the calculated results are summarized, along with the parameters used in the calculation. Figures 9 and 10 show the plots of the cross-sections

Table 2. Quenching Cross-Sections Calculated by a Collision Complex Model and the Parameters Used for the Calculation

Compounds	μ[a]	α[b]	IP[c]	σ_{1q}[d]	σ_{3q}[d]
NH(c¹Π)	1.70[e]	1.35[f]	7.48[g]		
NH(A³Π)	1.31[e]	1.35[f]	9.93[g]		
CH_4	0	2.60	12.6	55.8	56.2
C_2H_6	0	4.47	11.5	66.2	66.5
C_3H_8	0.084	6.29	11.10	78.3	77.5
c-C_3H_6	0	5.82	10.09	71.4	71.4
n-C_4H_{10}	0.050	8.42	10.63	83.7	83.2
i-C_4H_{10}	0.132	8.42	10.57	87.6	86.2
C_2H_4	0	4.26	10.50	64.6	64.7
C_3H_6	0.366	6.20	9.73	91.5	87.1
1-C_4H_8	0.34	8.14	9.63	96.2	92.3
i-C_4H_8	0.500	8.14	9.23	103.7	97.9
t-Δ^2-C_4H_8	0	8.14	9.13	79.1	78.7
c-Δ^2-C_4H_8	0.257[h]	8.14	9.13	91.8	88.6

a) Dipole moments in units of 3.3356×10^{-30} Cm; "CRC Handbook of Chemistry and Physics," 61st ed., CRC Press Inc., Boca Raton, (1980—1981), E-64, unless otherwise cited. b) Polarizabilities in units of 10^{-30} m³; estimated by the method described on p. 947 of Ref. 24, unless otherwise cited. c) Ionization potentials in units of 96.4846 kJ mol⁻¹; "CRC Handbook of Chemistry and Physics," 61st ed., CRC press Inc., Boca Raton, (1980—1981), E-69, unless otherwise cited. d) Calculated quenching cross sections in units of 10^{-16} cm². e) T. A. R. Irwin and F. W. Dalby, *Can. J. Phys.*, **43**, 1766 (1965). f) Assumed; see Ref. 19. g) Calculated from the ionization potential of NH($X^3\Sigma^-$) and the excitation energies of NH(c¹Π) and NH(A³Π). h) Chemical Society of Japan, Ed., "Kagaku Binran Kisohen," 3rd ed., Maruzen Tokyo (1984), II-719.

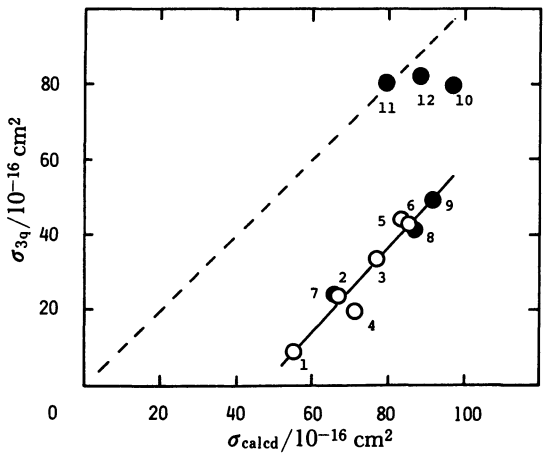

Fig. 9. Plots of the experimental cross sections, σ_{3q}, against those calculated by the collision complex model, σ_{calcd}, for quenching NH(A³Π). The numbers correspond to the compounds listed in Table 1.

observed against calculated ones. The observed cross-sections are smaller than the calculated ones except for higher olefins. Hofzumahaus and Stuhl evaluated the quenching probability $P=\sigma_{obsd}/\sigma_{calcd}$, to be about 0.3 by comparison with their results.[19] The results shown in Figs. 9 and 10, however, suggest that the probability depends on the molecular complexity.

Quenching Mechanism. In the case of O(¹D), the

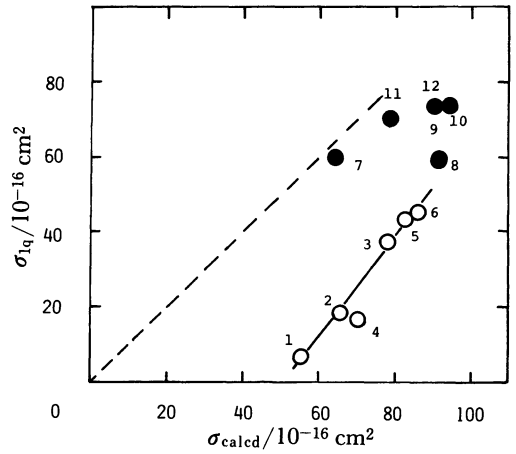

Fig. 10. Plots of the experimental cross sections, σ_{1q}, against those calculated by the collision complex model, σ_{calcd}, for quenching NH($c^1\Pi$). The numbers correspond to the compounds listed in Table 1.

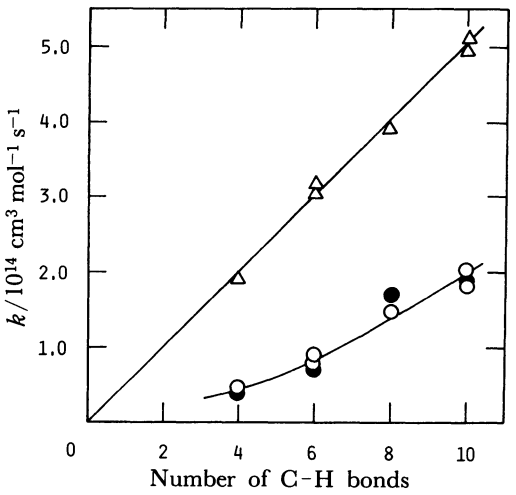

Fig. 11. Plots of reaction rates, k, against the number of C-H bonds included in paraffin. O: NH($A^3\Pi$), ●: NH($c^1\Pi$), and △: O(^{1}D).

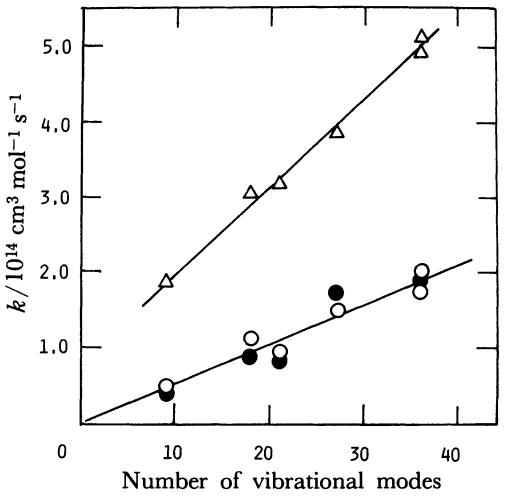

Fig. 12. Plots of reaction rates, k, against the number of vibrational modes of paraffin. O: NH($A^3\Pi$), ●: NH($c^1\Pi$), and △: O(^{1}D).

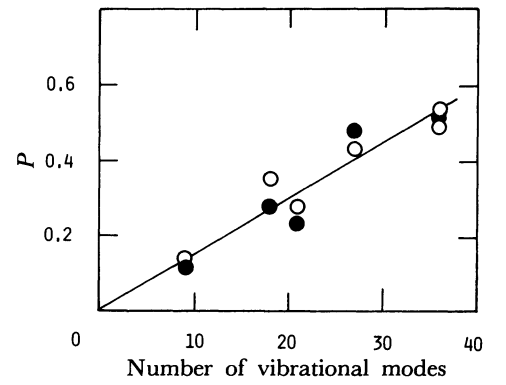

Fig. 13. Plots of quenching probabilities, P, against the number of vibrational modes of paraffin. O: NH($A^3\Pi$) and ●: NH($c^1\Pi$).

reaction rates of paraffin are known to be proportional to the number of C-H bonds included,[25] as is shown in Fig. 11. In the cases of the quenching of NH($A^3\Pi$) and NH($c^1\Pi$) by paraffin, the rate constants do not linearly increase with the number of C-H bonds included. This fact can not be explained by the term of the difference in the bond-dissociation energies, because n-C_4H_{10} quenches NH($A^3\Pi$) or NH($c^1\Pi$) as efficiently as i-C_4H_{10}, which has a weaker C-H bond than the former.

As is shown in Fig. 12, a good correlation was obtained between the quenching rates of paraffin and the number of the vibrational modes of quenchers in the cases of the quenching of NH($c^1\Pi$) and NH($A^3\Pi$). This fact may suggest that the intermolecular vibrational relaxation process in the collision complex is important. If the intermolecular vibrational relaxation is inefficient, the collision complex will decompose to the initial reactants; i.e., no quenching reactions will occur. That is, the quenching probability, P, becomes small for the molecules which have fewer vibrational modes. This trend is clearly shown in Fig. 13, where the quenching probabilities are plotted against the number of vibrational modes of the quenchers.

In the case of the quenching of NH($c^1\Pi$) by olefins, it is necessary to assign a large value of P, as may be seen from Fig. 10. A large value of P could not be explained by the term of the number of vibrational modes. In the above consideration, the rate of intermolecular vibrational relaxation is assumed to be an important factor in determining the probability. If the collision complex formed from olefin is considered to be tight enough for the efficient intermolecular vibrational relaxation, the collision probability will be high. Another possible explanation is that the rate of the decomposition to an exit channel is much faster than that of the returning to the initial reactants. At present, it is difficult to decide which mechanism is more important. The property of the collision complex is, in any event, an important factor in the quenching, although the validity of the assumption made for the

calculation of σ_{calcd} should be more carefully examined.

References

1) T. G. Slanger, "Reactions of Small Transient Molecules. Kinetics and Energetics," ed by A. Fontijin and M. A. A. Clyne, Academic Press, London (1983), p. 231.

2) S. Tsunashima, M. Hotta, and S. Sato, *Chem. Phys. Lett.*, **64**, 438 (1979); S. Tsunashima, J. Hamada, M. Hotta, and S. Sato, *Bull. Chem. Soc. Jpn.*, **53**, 2443 (1980); J. Hamada, S. Tsunashima, and S. Sato, *ibid.*, **55**, 1739 (1982); J. Kawai, S. Tsunashima, and S. Sato, *Nippon Kagaku Kaishi*, **1984**, 32.

3) S. Sato, T. Kitamura, and S. Tsunashima, *Chem. Lett.*, **1980**, 687; S. Tsunashima, T. Kitamura, and S. Sato, *Bull. Chem. Soc. Jpn.*, **54**, 2869 (1981).

4) T. Kitamura, S. Tsunashima, and S. Sato, *Bull. Chem. Soc. Jpn.*, **54**, 55 (1981); J. Hamada, S. Tsunashima, and S. Sato, *ibid.*, **56**, 662 (1983).

5) J. Kawai, S. Tsunashima, and S. Sato, *Chem. Phys. Lett.*, **110**, 655 (1984).

6) J. Kawai, S. Tsunashima, and S. Sato, *Bull. Chem. Soc. Jpn.*, **55**, 3312 (1983).

7) J. Kawai, S. Tsunashima, and S. Sato, *Chem. Lett.*, **1984**, 823.

8) O. Kajimoto and T. Fueno, *Chem. Phys. Lett.*, **80**, 484 (1981); O. Kondo, J. Miyata, O. Kajimoto, and T. Fueno, *Chem. Phys. Lett.*, **88**, 424 (1982).

9) S. Kodama, *Bull. Chem. Soc. Jpn.*, **56**, 2348 (1983); *ibid.*, **56**, 2355 (1983); *ibid.*, **56**, 2363 (1983); *ibid.*, **58**, 2891 (1985); *ibid.*, **58**, 2900 (1985).

10) A. P. Baronavski, R. G. Miller, and J. R. McDonald, *Chem. Phys.*, **30**, 119 (1978); J. R. McDonald, R. G. Miller, and A. P. Baronavski, *Chem. Phys.*, **30**, 133 (1978); W. S. Drozdoski, A. P. Baronavski, and J. R. McDonald, *Chem. Phys. Lett.*, **64**, 421 (1979); J. W. Cox, H. H. Nelson, and J. R. McDonald, *Chem. Phys.*, **96**, 175 (1985).

11) L. G. Piper, R. H. Krech, and R. L. Taylor, *J. Chem. Phys.*, **73**, 791 (1980).

12) B. Gelernt, S. V. Filseth, and T. Carrington, *J. Chem. Phys.*, **65**, 4940 (1976).

13) C. Zetsch and F. Stuhl, *J. Chem, Phys.*, **66**, 3107 (1977).

14) K. Schofield, *J. Photochem.*, **9**, 55 (1978).

15) H. Okabe, *J. Chem. Phys.*, **49**, 2726 (1968).

16) M. Kawasaki, Y. Hirata, and I. Tanaka, *J. Chem. Phys.*, **59**, 648 (1973).

17) N. Nishi, H. Shinohara, and J. Hanazaki, *Rev. Laser Eng.*, **10**, 394 (1982).

18) H. K. Haak and F. Stuhl, *J. Phys. Chem.*, **88**, 2201 (1984); *ibid.*, **88**, 3687 (1984).

19) A. Hofzumahaus and F. Stuhl, *J. Chem. Phys.*, **82**, 3152 (1985).

20) S. Sasaki, S. Tsunashima, and S. Sato, *Bull. Chem. Soc. Jpn.*, **59**, 1671 (1986).

21) D. H. Stedman, *J. Chem. Phys.*, **52**, 3966 (1970).

22) P. W. Fairchild, G. P. Smith, D. R. Crosley, and J. B. Jeffries, *Chem. Phys. Lett.*, **107**, 181 (1984).

23) H. M. Lin, M. Seaver, K. Y. Tang, A. E. W. Knight, and C. S. Parmenter, *J. Chem. Phys.*, **70**, 5442 (1979); C. S. Parmenter and M. Seaver, *ibid.*, **70**, 5458 (1979).

24) J. O. Hirschfelder, C. F. Curtiss, and R. B. Bird, "Molecular Theory of Gases and Liquids," 2nd ed., Wiley, London (1964).

25) P. Michaud, G. Paraskevopoulos, and R. J. Cvetanović, *J. Phys. Chem.*, **78**, 1457 (1974).